Journal of Vacuum Science & Technology A

Intrinsic and Atomic Layer Etching Enhanced Area-Selective Atomic Layer Deposition of Molybdenum Disulfide Thin Films

Jake Soares[1], Wesley Jen[1], John D. Hues[1], Drew Lysne[1], Jesse Wensel[2], Steven M. Hues[1], Elton Graugnard[1,3,a)]

[1] Micron School of Materials Science and Engineering, Boise State University, 1910 University Dr., Boise, ID 83725, USA
[2] Micron Technology, 8000 S Federal Way, Boise, ID, 83707, USA
[3] Center for Advanced Energy Studies, Idaho Falls, ID 83401, USA

a) Electronic mail: eltongraugnard@boisestate.edu

For continual scaling in microelectronics, new processes for precise high volume fabrication are required. Area-selective atomic layer deposition (ASALD) can provide an avenue for self-aligned material patterning and offers an approach to correct for edge placement errors commonly found in top-down patterning processes. Two-dimensional transition metal dichalcogenides (TMDs) also offer great potential in scaled microelectronic devices due to their high mobilities and few-atom thickness. In this work, we report ASALD of MoS_2 thin films by deposition with MoF_6 and H_2S precursor reactants. The inherent selectivity of the MoS_2 atomic layer deposition (ALD) process is demonstrated by growth on common dielectric materials in contrast to thermal oxide/ nitride substrates. The selective deposition produced few layer MoS_2 films on patterned growth regions as measured by Raman spectroscopy and time-of-flight secondary ion mass spectrometry. We additionally demonstrate that the selectivity can be enhanced by implementing atomic layer etching (ALE) steps at regular intervals during MoS_2 growth. This area-selective ALD process provides an approach for integrating 2D films into next-generation devices by leveraging the

inherent differences in surface chemistries and providing insight in the effectiveness of a supercycle ALD and ALE process.

I. INTRODUCTION

As feature sizes shrink, the need for precise patterning methods is critical. Commonly, top-down approaches to nanoscale processing are used to pattern features in high volume manufacturing (HVM) of semiconductor devices. These include photolithography,[1, 2, 3] and other soft-lithography techniques[4, 5] followed by dry etching,[6] wet etching,[7] or deposition. These methods have been a standard in semiconductor manufacturing; however, as dimensions scale below the 7 nm node,[8] new techniques need to be developed to correct for misalignment issues.[9] At the nanoscale, pattern misalignments can have a drastic impact on device performance and even lead to device failure. This issue is only exacerbated when the number of processing steps, comprising further patterning and deposition, build upon the misaligned underlying layer.

Area-selective atomic layer deposition (ASALD) can mitigate alignment errors by providing a bottom-up approach to selectively deposit films on predetermined areas.[10] This method uses the differences in surface chemistry between growth (GA) and non-growth (NGA) areas to deposit primarily on surfaces that promote nucleation. ALD is a technique that employs self-limiting surface chemical reactions for thin film growth. While sometimes valued as a deposition process that produces continuous, pinhole-free conformal thin films,[11] that deposition behavior relies on uniform surface chemistry to promote uniform film nucleation. However, by exploiting the differences in surface chemistry, preferential nucleation can promote selectivity during deposition.[12]

Several methods have been reported to enable ASALD.[13] Self-assembled monolayers (SAMs) have been shown to promote selectivity by selectively functionalizing (or

defunctionalizing) a specific area on a pre-pattered substrate.[14-16] SAMs achieve this selectivity due to the tail group (functionalized group) of the monolayer, which blocks precursor chemisorption on the substrate surface. Precursor choice also influences ALD selectivity by means of ligand reactivity and ligand size, as shown in the selective deposition of Al_2O_3 on SiO_2.[17] This method is useful for defining both growth and non-growth regions; however, it typically relies on a wet chemistry and long exposures for SAM placement and ordering. Using small molecule inhibitors that selective bind to patterned regions can yield ASALD processes where the inhibitor exposure can form a third step in an ALD cycle.[18] Lastly, selective deposition can be achieved by exploiting inherent substrate selectivity based on substrate functional groups. Some of these methods rely on precursor adsorption reactivity.[19, 20] This approach has been demonstrated by the implementation and control over nucleation islands for selective plasma-enhanced ALD of WS_2 and by control over the density of hydroxyl (OH) groups on SiO_2 surfaces for the selective deposition of MoS_2.[21, 22, 23] These processes require use of a pre-patterning step for seed or OH placement, for example, using either O_2 plasma[21] or ion beam patterning.[22] To our knowledge there has been only one other ASALD report of selective deposition of MoS_2 films by use of assisted etching during deposition. Ahn *et al*. has demonstrated the ASALD of MoS_2 by $MoCl_5$ adsorption and subsequent self-etching effect for selective MoS_2 deposition on Al patterns versus SiO_2.[24]

In this work, we report area-selective ALD of MoS_2 thin films by deposition with MoF_6 and H_2S reactants. The inherent differences in surface groups between common ALD-deposited metal oxide surfaces and thermal oxide/nitride substrates leads to the selective nucleation and deposition of MoS_2 films on the metal oxide regions. Initial screening of substrate materials by X-ray photoelectron spectroscopy (XPS) identified materials that either promoted or inhibited

Journal of Vacuum Science & Technology A

nucleation of MoS_2 after a range of MoS_2 cycles. Selectivity parameters were calculated between growth and non-growth surfaces. Substrate templates were then pre-pattered with both growth and non-growth areas to verify the selective MoS_2 process. Time-of-flight secondary ion mass spectrometry (ToF-SIMS) and Raman mode line maps confirmed selective MoS_2 deposition on growth regions of the template substrates. Further, selectivity was enhanced by integrating atomic layer etching steps during ALD.

II. EXPERIMENTAL

A. MoS_2 deposition

ALD growth of MoS_2 films were performed in custom viscous flow reactor following the process reported previously.[25] Briefly, the process pressure was held constant at ~1 Torr by flowing 125 sccm of ultra-high purity nitrogen (99.99% Norco) as a carrier gas. Reactor temperatures were held at 200 ^oC. MoS_2 ALD process followed typical dosing scheme of t_1-t_2-t_3-t_4, where exposure times are in seconds. t_1 and t_2 denote the molybdenum hexafluoride (molybdenum(VI) fluoride, Fisher Scientific) dose and purge times. t_3 and t_4 denote the H_2S (hydrogen Sulfife, 99.5+%, Millipore Sigma) dose and purge times. Partial pressures of reactants for each dose were 60 mTorr for MoF_6 and 400 mTorr for H_2S. Due to the high pressures of H_2S, a regulator set at 1 ATM, and 200 μm orifice was placed on the H_2S manifold delivery line.

Coupon substrates for MoS_2 ALD consisted of Si(100) with a native oxide or with an ALD dielectric coating. Deposited dielectrics consisted of alumina (Al_2O_3), hafnia (HfO_2), and titania (TiO_2) using trimethylaluminum (TMA, Millipore Sigma), tetrakis(dimethylamido)hafnium(IV) (TDMAH, 98% (99.99%-Hf), Millipore Sigma), and titanium tetrachloride ($TiCl_4$, 99.995%, Millipore Sigma), respectively. For each dielectric, the oxygen source was water. Other coupon substrates included a 300 nm thermal SiO_2 (University

Wafer) and SiN and SiO_xN_y substrates (Micron Technology). Prior to any deposition, samples were sonicated for 1 min in acetone and 1 min in ethanol and then rinsed in Nanopure water. Lastly, samples were subject to a plasma glow discharge chamber for 30 seconds at a pressure of ~2 Torr in air to remove residual hydrocarbons.

Template substrates were patterned through standard photolithography. Coupons of doped silicon with 300 nm thermal oxide SiO_2 or SiO_xN_y were cleaved and cleaned with acetone and ethanol to remove any debris or contaminants during the cleaving process. The substrates were then placed on a spin-coater and coated with hexamethyldisilazane (HDMS) as a photoresist adhesion promoter and SPR220 3.0 (Megaposit) as the photoresist. A soft-bake at 115 °C for 90 seconds was conducted following each coating step. The coated substrates were aligned to a photomask and exposed using a Quintel Q-4000 Contact Aligner. The samples were subsequently developed using a photoresist developer (TMAH, Megaposit MF-26A) and rinsed with deionized water. Once dry, the patterned samples were placed in a GEMStar XT thermal ALD system (Arradiance) for deposition of a metal oxide film. Once the metal oxide was deposited, the photoresist was removed by sonicating the template substrate in acetone, followed by the cleaning process described earlier.

B. Characterization

X-ray photoelectron spectroscopy (XPS) measurements were performed using a Physical Electronics (PHI) 5600 ESCA system using a monochromated Al K-alpha source with an analysis area of 3 mm × 10 mm. Survey scans used a pass energy of 200 eV and step size of 1 eV. High resolution scans used a pass energy of 50 eV and step size of 0.1 eV. The XPS data were analyzed using MultiPak 9.6. All spectra were referenced to the 1s peak (284.8 eV) of

adventitious carbon. Peak fitting of all high-resolution scans utilized a Shirley background to define the baseline. Region bounds were chosen such that bounds encompassed the totality of peaks present and were extended as far as possible without overlapping with other chemical peaks nearby. A Gaussian-Lorentzian peak mix was used when fitting spectra.

Raman spectroscopy was conducted on a Horiba LabRAM system in reflection mode. A 532 nm excitation laser, using a 100× aperture was used to probe samples. A neutral density filter setting ranging from 25% was used to prevent damage to the MoS_2 samples. Spectra were acquired over the 360-440 cm^{-1} range to capture crystalline MoS_2 modes. Line scans were analyzed over the range of 395-415 cm^{-1} to capture the MoS_2 A_{1g} peak area.

Atomic force microscopy measurements (AFM) were performed on a MultiMode 8 (Bruker) operating in PeakForce-QNM mode. ScanAsyst-Air-HR probes (Bruker) with a tip radius of 2 nm were used for imaging. Image processing was carried out in NanoScope Analysis 2.0.

In this work, ToF-SIMS images were acquired by measuring the intensity of each analyte, at given mass/charge, at each pixel to provide a distribution of the analyte across the surface. Analyses were performed in positive secondary ion mode using a 25 keV Bi_1^+ primary ions beam rastered over a 200 × 200 μm^2 area with an original image pixel density of 512 × 512, images were then binned to 128 × 128, post analysis, to improve contrast.

III. RESULTS AND DISCUSSION

A. Material screening

Initial screening of various substrate materials was experimentally conducted to identify substrates that promoted or inhibited MoS_2 growth. We expected that substrates with larger hydroxyl (OH) concentrations would promote deposition compared to substrates that have strong

surface bonding and lack reactive surface groups. Our previous studies have shown a temperature dependence for MoF_6 precursor adsorption, which we attribute to differences in relative hydroxyl concentrations.[26] These studies suggest that increased OH concentrations promote increases in MoF_6 chemisorption on metal oxide surfaces. Moreover, Lawson *et al*. reported density functional theory calculations describing the nucleation behavior of MoF_6 precursors on hydroxylated and non-hydroxylated metal oxide surfaces. [27] They reported a higher reactivity and subsequent chemisorption of the MoF_6 precursor towards the hydroxylated metal oxides compared to a weak interaction with non-hydroxylated metal oxide surfaces.

To experimentally screen surfaces for MoS_2 nucleation, XPS spectra were acquired for planar coupon substrate materials after MoS_2 ALD. Each material substrate was exposed to 22 MoS_2 ALD cycles followed by annealing at 650 °C in H_2S for 30 min. After deposition, high-resolution Mo 3d XPS scans were captured (Fig. 1). The spectra are offset vertically for ease of viewing. The relative intensities of the spectra were used to determine which material surfaces promoted or delayed MoS_2 nucleation. Based on these preliminary experiments, thermal SiO_2 (TO) and SiO_xN_y had the lowest concentration of Mo compared to the metal oxides, such as Al_2O_3 and HfO_2, that showed greater Mo 3d peak intensities.

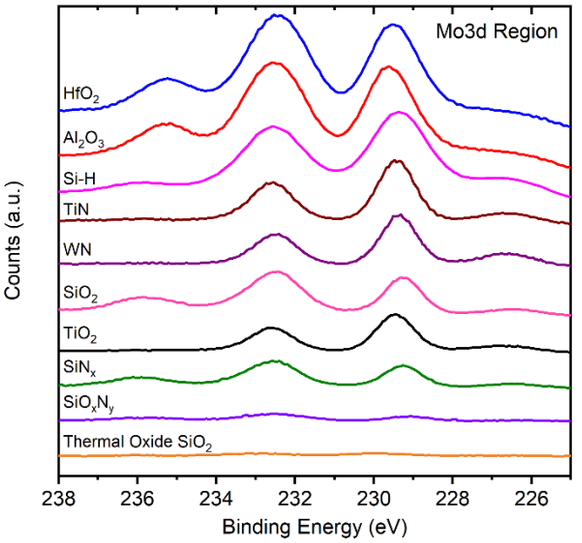

FIG. 1. X-ray photoelectron spectroscopy scans on a variety of substrate surfaces measuring photo-emitted electron intensities in the Mo 3d region after 22 MoS_2 cycles at 200 °C and annealing at 650 °C for 30 min. Spectra are offset vertically for clarity. These data enable identification of surfaces that either promote (HfO_2 and Al_2O_3) or inhibit (SiN_x, SiO_xN_y and thermal oxide SiO_2) MoS_2 nucleation.

Based on the XPS data, additional experiments were conducted to measure the selectivity between the surfaces that exhibited large differences in Mo concentration. ALD Al_2O_3 and HfO_2 were identified as materials that promoted MoS_2 growth, while SiN_x, SiO_xN_y, and TO were seen as substrates that delayed nucleation. ALD MoS_2 was performed on planar coupons of the respective substrate materials. After 5-20 MoS_2 ALD cycles, high-resolution XPS scans were taken on the coupons over the Mo 3d region. Peak fitting of the spectra within the Mo 3d region was conducted to calculate the integrated area. These calculations excluded the overlapping S 2s peak area. Figure 2 shows the Mo peak area versus the number of ALD cycles for each substrate. A clear Mo nucleation delay can be seen for the TO (squares), SiN_x (diamonds), and SiO_xN_y substrates (inverted triangles) compared to the metal oxides Al_2O_3 (circles) and HfO_2 (triangles).

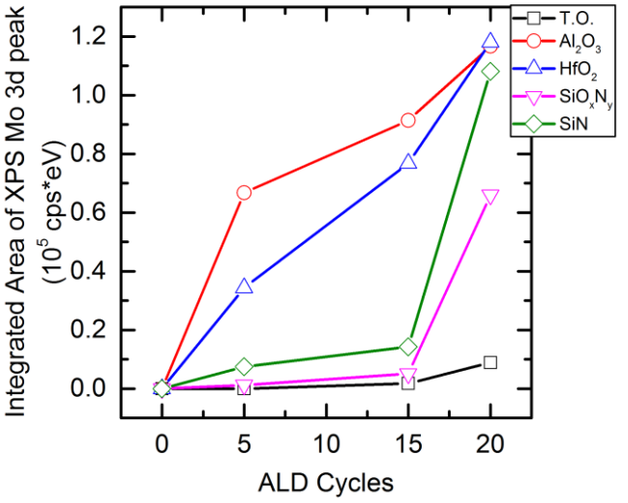

FIG. 2. Integrated area of XPS Mo 3d peak region as a function of MoS_2 ALD cycles for a variety of substrates. All substrates were prepared with 20 cycles of MoS_2 ALD at 200 °C. Integrated area was calculated after peak fitting the Mo 3d region (excluding the overlapping S 2s spectra).

From the XPS results of the Mo 3d integrated peak area, the selectivity between the growth and non-growth areas was calculated using Equation 1. The selectivity is based on the amount of material present after deposition on growth areas (θ_{GA}) and non-growth areas (θ_{NGA}). [28]

$$Selectivity = \frac{\theta_{GA} - \theta_{NGA}}{\theta_{GA} + \theta_{NGA}} \qquad (1)$$

Figure 3 shows the calculated selectivity values as a function of ALD cycles between identified growth and non-growth surfaces. The Al_2O_3 and TO had the greatest Mo concentration differences. After 5 MoS_2 cycles there was a high selectivity value of S = ~1. Essentially no Mo was detected on the TO surface by XPS. The selectivity was calculated to be S = 0.96 at 15 cycles and decreased to S = 0.85 at 20 ALD cycles. Beyond 20 cycles, the selectivity dropped dramatically to S = 0.51 for 30 ALD cycles.

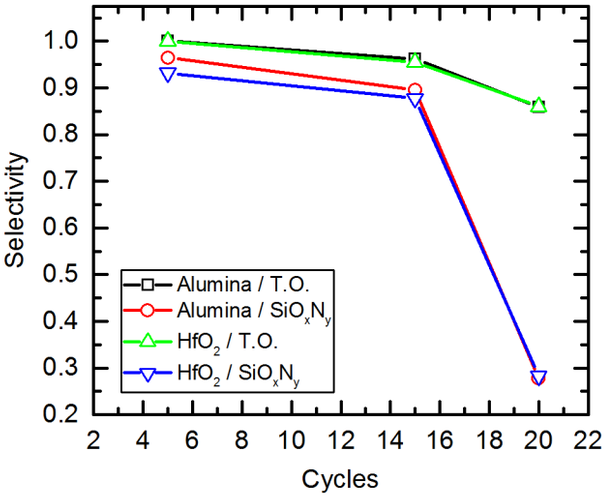

FIG. 3. Calculated selectivity parameter as a function of MoS_2 ALD cycles at 200 °C for blanket substrates that promote or inhibit MoS_2 growth. The selectivity was calculated based on integrated XPS Mo concentrations.

The high selectivity observed between the Al_2O_3 and the TO is expected due to relative concentrations of surface OH groups. It has been reported that ALD alumina films (deposited with TMA and H_2O) contain high concentrations of OH groups throughout the film[29] and are the terminating groups left on the surface after deposition (H_2O as last precursor dose).[30] Studies have also experimentally calculated the hydroxyl coverage on the alumina surface and is expected to be ~9 nm^{-2} at 200 °C.[31] Comparatively, thermal oxide only has ~1.5-3 nm^{-2} OH group coverage.[32] This stark difference in OH concentration supports the observed selectivity between the TO and Al_2O_3 surfaces. Thermal oxide has also been shown to be relatively resistant to WF_6 nucleation during W chemical vapor deposition (CVD) and ALD reactions.[33, 34] In studies of selective W deposition, the presence of Si-OH groups was shown to contribute to nucleation on the non-growth SiO_2 surface. The fluorination on the SiO_2 surface can also play a role in either promoting or inhibiting nucleation[33] and can contribute to etching of SiO_2, which can extend selectivity.[34] To determine whether fluorination was inhibiting nucleation on the TO

surface, we performed 10 cycles of MoS_2 ALD, with no annealing, on ALD alumina, thermal SiO_2, and native SiO_2 cleaned in fuming sulfuric acid. The concentrations of Mo, S, and F are provided in the Supplemental Material (SM) at [URL will be inserted by AIP Publishing]. The alumina and native SiO_2 exhibit Mo and S content, indicating nucleation, and fluorine content is expected from residual fluorine within the unannealed films. However, the thermal SiO_2 exhibited negligible Mo and S content. The results indicate a small level of fluorination from the MoF_6 exposures to the TO substrate, but additional studies are needed to evaluate whether this fluorine is inhibiting the nucleation of Mo or whether the Mo nucleation is inhibited primarily by the lack of hydroxyl groups.

B. ASALD on Templates

To further explore the selective process, template surfaces were created that contained both a growth area and non-growth area. TO, SiN_x, and SiO_xN_y substrates were patterned with ALD Al_2O_3, HfO_2 or TiO_2 using photolithography. Templates were then exposed to 20 MoS_2 ALD cycles at 200 °C followed by annealing at 650 ºC in H_2S for 30 min to form crystalline films. [35] The samples were then characterized by Raman spectroscopy to probe the selectivity of the deposition process.

Raman point scans were captured on and off the growth regions for each template substrate. See the SM for additional Raman mode line scans and ToF-SIMS maps. Figure S1 in the SM shows the results of point scans on Al_2O_3/TO and Al_2O_3/SiO_xN_y templates. Characteristic E^1_{2g} and A_{1g} modes[36] for crystalline MoS_2 were identified on the growth region (Al_2O_3) for both template substrates. These modes can be identified at ~380 and 405 cm^{-1}. No modes were observed on the non-growth TO regions, while a slight emergence of the A_{1g} mode on the

SiO_xN_y non-growth region was observed. With the initial results from point scans, Raman line scans of the A_{1g} mode intensity were conducted across a ~10 μm growth area feature for all templates. The line scans spanned far enough to include regions of the non-growth areas (TO or SiO_xN_y). These Raman line scans are shown in Figure 4(a). An optical image of and Al_3O_3 / TO sample is shown in Figure 4(b). The annotated dashed line represents where the line scan was taken across the template substrate. All templates show great contrast between the growth and non-growth regions revealing a high A_{1g} intensity within the growth areas only. For all patterned growth areas, the Raman A_{1g} mode intensity was roughly ~2 orders of magnitude larger than compared to the TO substrate. The morphology of the interface between the Al_2O_3 and TO regions was investigated using AFM following 20 cycles of MoS_2 ALD and annealing in H_2S for 30 min at 650 °C. Figure S3 shows greater deposition on the Al_2O_3 region but also reveals MoS_2 nuclei forming on the TO region. We attribute the eventual loss of selectivity to the coalescence of the MoS_2 nuclei in the TO region with additional ALD cycles.

The selectivity was also probed on SiO_xN_y and SiN_x substrates patterned with ALD Al_2O_3. These also show a degree of selectivity, although it is not as pronounced as the Al_2O_3/TO. This result can be expected as the previous XPS data indicates a lower calculated selectivity with addition to the slight emergence of the A_{1g} mode captured in the Raman point scan. The Raman data for the templates prepared with SiO_xN_y and SiN_x can be found in the SM.

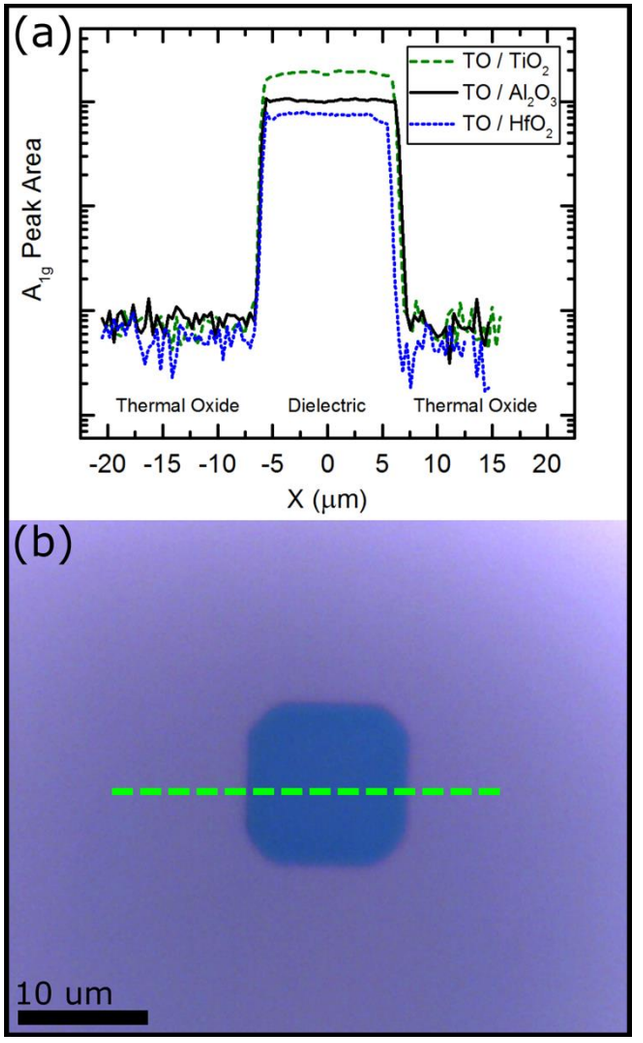

FIG. 4. (a) Raman line scans across the template substrates containing both growth and non-growth regions. Intensity is measured by crystalline MoS_2 A_{1g} peak area. Clear indication of crystalline MoS_2 can be identified on all growth areas. (b) Example optical image of a patterned Al_2O_3 / TO region. The dashed line approximates the region of the line scan across the template. Samples were prepared with 20 cycles of MoS_2 ALD at 200 °C followed by annealing in H_2S at 650 °C for 30 min.

To further characterize the selectivity of the ASALD process, time-of-flight secondary ion mass spectrometry (ToF-SIMS) elemental maps of template substrates were acquired.

Template substrates for these measurements were made of either TO or SiO_xN_y substrates patterned with ALD Al_2O_3. Templates were prepared with 20 cycles of MoS_2 ALD at 200 °C and were annealed at 650 ºC in H_2S for 30 min. to form a crystalline film. Figure 5 shows the Mo^+, $SiOH^+$, and Al^+ elemental channels from ToF-SIMS analysis. The intensity describes the elemental (mass/charge) concentration of the listed species. Both growth and non-growth regions can easily be identified by the relative color scale of the respective ion species. The Mo^+ channel clearly distinguishes the selectivity of the molybdenum species on the Al_2O_3 growth area. Where the Mo^+ intensity is greatest within the central growth area and near zero on the surrounding TO substrate. ToF-SIMS maps showing similar results for selective deposition on the Al_2O_3/SiO_xN_y patterned samples can be found in the SM.

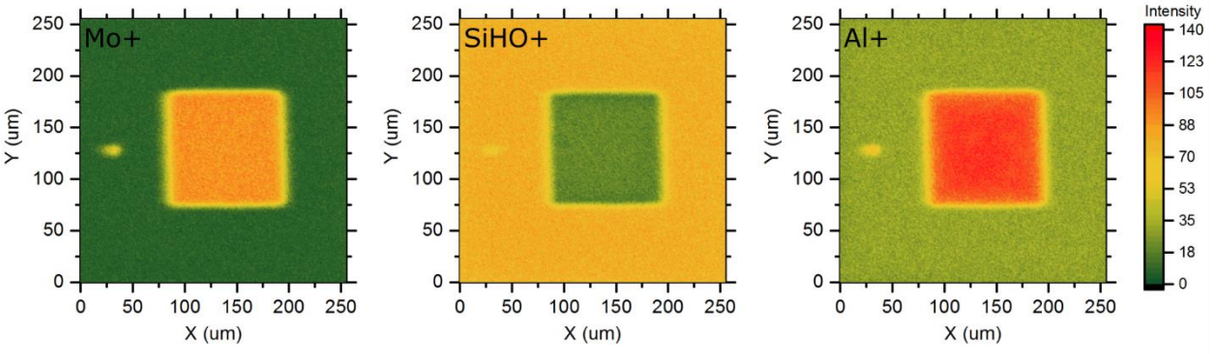

FIG. 5. Time-of-flight secondary ion mass spectrometry maps of alumina / TO template following 20 MoS_2 ALD cycles at 200 °C. Maps show clear selectivity of Mo within the patterned alumina growth area. Essentially no Mo is present on the non-growth thermal oxide area.

C. Etching Enhanced ASALD of MoS_2

Recently, several groups have reported the successful combination of ASALD and selective etching to improve process selectivity.[37-40] These works integrate etching steps within

the ALD process to suppress the nucleation that occurs on the non-growth areas. By incorporating intermittent etching steps during ALD, the selectivity between the growth and non-growth areas can effectively be extended. We have previously reported an atomic layer etching (ALE) process for MoS_2 thin films.[41] This ALE process utilizes the sequential exposure of MoF_6 and H_2O precursors for MoS_2 film removal. This ALE process was incorporated to extend the selectivity of the MoS_2 ASALD process.

Deposition enhanced by etching was investigated on blanket planar coupons of Al_2O_3 and TO. We implemented supercycle recipes for these experiments, where one supercycle is defined as a number of ALD cycles followed by a number of ALE cycles. At intervals of every 10 ALD cycles, 30 cycles of etching were performed, comprising one supercycle. A total of 2-3 supercycles were conducted on the coupon substrates to test the etching assisted ASALD process.

The integrated area of XPS Mo 3d data shows a much lower Mo concentration after 20 and 30 ALD cycles for deposition that implemented a supercycle recipe as compared to the standard ASALD process (Fig. 6). The resulting selectivity was calculated for the experiments utilizing supercycle recipes producing $S_{(SC\ x2)} = 0.95$ and $S_{(SC\ x3)} = 0.92$ after a total of 20 and 30 ALD cycles, respectively. These data suggest that implementing a dep-etch supercycle recipe can suppress Mo nucleation on the non-growth region over an extended range of ALD cycles. This result can be implemented to obtain a much more selective deposition process by reducing any formed nuclei on the non-growth region, and aid in the selective deposition of thicker MoS_2 films.

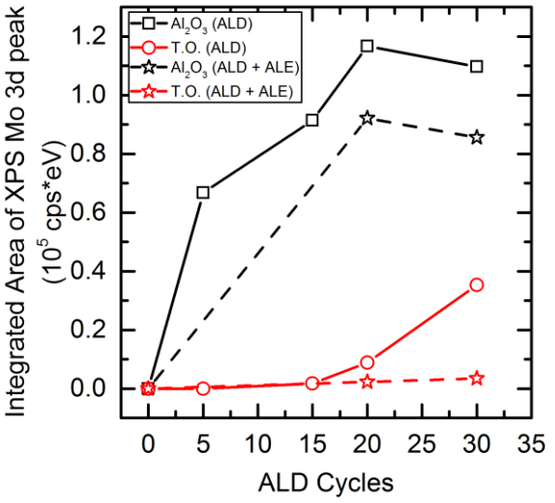

FIG. 6. Integrated area of XPS Mo 3d peak region as a function of total MoS_2 ALD cycles for thermal oxide and Al_2O_3 substrates. The incorporation of etching steps is shown to decrease the amount of Mo present after a total of 20 and 30 ALD cycles. Dashed lines indicate growth that integrated supercycles of deposition and etching. Solid lines indicate ASALD without ALE supercycles.

IV. CONCLUSIONS

In this work, we report the ASALD of MoS_2 films. Initial screening of common semiconductor surfaces including metal oxides and silicon oxide/nitride was conducted by XPS measurements. A nucleation delay was observed on thermal SiO_2 and SiN_x and SiO_xN_y substrates compared to Al_2O_3 and HfO_2. This nucleation delay is attributed to a difference in inherent hydroxyl concentrations between the surfaces, which impacts the nucleation of the MoF_6 precursor. The selectivity parameter was calculated between substrates that delayed nucleation and promoted nucleation. A selectivity between thermal SiO_2 and Al_2O_3 was calculated to be S = 0.85 after 20 ALD cycles. Time-of-flight SIMS and Raman line scans confirmed the ASALD process of MoS_2 on pre-patterned template substrates of Al_2O_3 and thermal SiO_2. The selectivity of our ASALD process was improved by implementing atomic layer etching steps during ALD. This combination of

Journal of Vacuum Science & Technology A

deposition and etching extended the total number of ALD cycles that could be performed while improving the selectivity between surfaces. This work will help realize the potential for area-selective ALD by utilizing inherent differences in substrate surface chemistry. Additionally, this study demonstrates processing methods that can be used for MoS_2 integration in manufacturing and offers an approach to bottom-up, self-aligned fabrication.

ACKNOWLEDGMENTS

We would like to thank members of the Atomic Films Lab for valuable discussions. We thank Icelene Leong for valuable assistance with the XPS studies. We thank Scott Sills at Micron Technology for providing coated wafers for blanket studies. Atomic force microscopy was performed in the Surface Science Laboratory at Boise State University. This work was supported in part by National Science Foundation CAREER grant no. 1751268 and the National Science Foundation Center for Atomically Thin Multifunctional Coatings (ATOMIC) IUCRC (grant no. 2113873).

AUTHOR DECLARATIONS

Conflict of Interest

The authors have no conflicts to disclose.

SUPPLEMENTAL MATERIAL

Supplemental material at [URL will be inserted by AIP Publishing] for additional Raman spectra, an atomic force micrograph at a template edge, additional ToF-SIMS maps, and additional XPS data.

DATA AVAILABILITY

The data that support the described findings are available within the primary article and the supplemental material.

REFERENCES

1. G. E. Moore, presented at the Integrated Circuit Metrology, Inspection, and Process Control IX, (1995).
2. R. Seisyan, Technical Physics 56 (8), 1061-1073 (2011).
3. A. Pimpin and W. Srituravanich, Engineering Journal 16 (1), 37-56 (2012).
4. Y. Xia and G. M. Whitesides, Annual Review of Materials Science 28 (1), 153-184 (1998).
5. F. Wisser, B. Schumm, G. Mondin, J. Grothe and S. Kaskel, Journal of Materials Chemistry C 3 (12), 2717-2731 (2015).
6. K. Nojiri, Dry Etching Technology for Semiconductors. (Springer, 2015).
7. J. C. Love, K. E. Paul and G. M. Whitesides, Adv. Mater. 13 (8), 604-607 (2001).
8. A. Pandey, Silicon, 1-12 (2022).
9. R. Clark, K. Tapily, K.-H. Yu, T. Hakamata, S. Consiglio, D. O'Meara, C. Wajda, J. Smith and G. Leusink, Applied Physics Letters Materials 6 (5), 058203 (2018).
10. G. N. Parsons and R. D. Clark, Chem. Mater. 32 (12), 4920-4953 (2020).
11. S. M. George, Chem. Rev. 110 (1), 111-131 (2010).
12. A. Mackus, A. Bol and W. Kessels, Nanoscale 6 (19), 10941-10960 (2014).
13. A. J. M. Mackus, M. J. M. Merkx and W. M. M. Kessels, Chem. Mater. 31 (1), 2-12 (2019).
14. X. Jiang and S. F. Bent, J. Phys. Chem. C 113 (41), 17613-17625 (2009).

15. E. Färm, M. Vehkamäki, M. Ritala and M. Leskelä, Semiconductor Science and Technology 27 (7), 074004 (2012).
16. T.-L. Liu and S. F. Bent, Chem. Mater. 33 (2), 513-523 (2021).
17. I.-K. Oh, T. E. Sandoval, T.-L. Liu, N. E. Richey and S. F. Bent, Chem. Mater. 33 (11), 3926-3935 (2021).
18. A. Mameli, M. J. M. Merkx, B. Karasulu, F. Roozeboom, W. M. M. Kessels and A. J. M. Mackus, ACS Nano 11 (9), 9303-9311 (2017).
19. R. C. Longo, S. McDonnell, D. Dick, R. M. Wallace, Y. J. Chabal, J. H. Owen, J. B. Ballard, J. N. Randall and K. Cho, Journal of Vacuum Science & Technology B 32 (3), 03D112 (2014).
20. S. E. Atanasov, B. Kalanyan and G. N. Parsons, J. Vac. Sci. Technol. A 34 (1), 01A148 (2016).
21. B. Groven, Y. Tomczak, M. Heyns, I. Radu, and A. Delabie, J. Appl. Phys. 128, 175302 (2020).
22. X. Chen, Y. J. Park, T. Das, H. Jang, J.-B. Lee and J.-H. Ahn, Nanoscale 8 (33), 15181-15188 (2016).
23. S. F. Bartolucci, D. Kaplan and J. A. Maurer, 2D Materials 4 (2), 021017 (2017).
24. W. Ahn, H. Lee, H. Kim, M. Leem, H. Lee, T. Park, E. Lee and H. Kim, Phys. Status Solidi RRL 15 (2), 2000533 (2021).
25. A. U. Mane, S. Letourneau, D. J. Mandia, J. Liu, J. A. Libera, Y. Lei, Q. Peng, E. Graugnard and J. W. Elam, J. Vac. Sci. Technol. A 36 (1), 01A125 (2017).
26. J. Soares, S. Letourneau, M. Lawson, A. U. Mane, Y. Lu, Y. Wu, S. M. Hues, L. Li, J. W. Elam and E. Graugnard, J. Vac. Sci. Technol. A 40 (6), 062202 (2022).

27. M. Lawson, E. Graugnard and L. Li, Appl. Surf. Sci. 541, 148461 (2021).

28. W. L. Gladfelter, Chem. Mater. 5 (10), 1372-1388 (1993).

29. A. Dillon, A. Ott, J. Way and S. George, Surf. Sci. 322 (1-3), 230-242 (1995).

30. R. L. Puurunen, Journal of Applied Physics 97 (12) (2005).

31. R. A. Wind and S. M. George, J. Phys. Chem. A 114 (3), 1281-1289 (2010).

32. A. M. Hoyas, C. Whelan, J. Schuhmacher, J. Celis and K. Maex, Electrochemical and Solid-State Letters 9 (7), F64 (2006).

33. K. M. Chang, S. W. Wang, C. H. Li, J. Y. T. J. Y. Tsai and T. H. Y. T. H. Yeh, Jpn. J. Appl. Phys. 35 (12S), 6555 (1996).

34. P. C. Lemaire, M. King and G. N. Parsons, J. Chem. Phys. 146 (5), 052811 (2017).

35. S. Letourneau, M. J. Young, N. M. Bedford, Y. Ren, A. Yanguas-Gil, A. U. Mane, J. W. Elam and E. Graugnard, ACS Appl. Nano Mater. 1 (8), 4028-4037 (2018).

36. H. Li, Q. Zhang, C. C. R. Yap, B. K. Tay, T. H. T. Edwin, A. Olivier and D. Baillargeat, Adv. Funct. Mater. 22 (7), 1385-1390 (2012).

37. M. F. Vos, S. N. Chopra, M. A. Verheijen, J. G. Ekerdt, S. Agarwal, W. M. Kessels and A. J. Mackus, Chem. Mater. 31 (11), 3878-3882 (2019).

38. S. K. Song, H. Saare and G. N. Parsons, Chem. Mater. 31 (13), 4793-4804 (2019).

39. H. Saare, S. K. Song, J.-S. Kim and G. N. Parsons, J. Appl. Phys. 128 (10), 105302 (2020).

40. R. Vallat, R. Gassilloud, B. Eychenne and C. Vallée, J. Vac. Sci. Technol. A 35 (1), 01B104 (2017).

41. J. Soares, A. U. Mane, D. Choudhury, S. Letourneau, S. M. Hues, J. W. Elam and E. Graugnard, Chem. Mater. 35 (3), 927–936 (2023)

Journal of Vacuum Science & Technology A

Figure Captions

FIG. 1. X-ray photoelectron spectroscopy scans on a variety of substrate surfaces measuring photo-emitted electron intensities in the Mo 3d region after 22 MoS_2 cycles at 200 °C and annealing at 650 ºC for 30 min. Spectra are offset vertically for clarity. These data enable identification of surfaces that either promote (HfO_2 and Al_2O_3) or inhibit (SiN_x, SiO_xN_y and thermal oxide SiO_2) MoS_2 nucleation.

FIG. 2. Integrated area of XPS Mo 3d peak region as a function of MoS_2 ALD cycles for a variety of substrates. All substrates were prepared with 20 cycles of MoS_2 ALD at 200 °C. Integrated area was calculated after peak fitting the Mo 3d region (excluding the overlapping S 2s spectra).

FIG. 3. Calculated selectivity parameter as a function of MoS_2 ALD cycles at 200 °C for blanket substrates that promote or inhibit MoS_2 growth. The selectivity was calculated based on integrated XPS Mo concentrations.

FIG. 4. (a) Raman line scans across the template substrates containing both growth and non-growth regions. Intensity is measured by crystalline MoS_2 A_{1g} peak area. Clear indication of crystalline MoS_2 can be identified on all growth areas. (b) Example optical image of a patterned Al_2O_3 / TO region. The dashed line approximates the region of the line scan across the template. Samples were prepared with 20 cycles of MoS_2 ALD at 200 °C followed by annealing in H_2S at 650 °C for 30 min.

FIG. 5. Time-of-flight secondary ion mass spectrometry maps of alumina / TO template following 20 MoS_2 ALD cycles at 200 °C. Maps show clear selectivity of Mo within the

patterned alumina growth area. Essentially no Mo is present on the non-growth thermal oxide area.

FIG. 6. Integrated area of XPS Mo 3d peak region as a function of total MoS_2 ALD cycles for thermal oxide and Al_2O_3 substrates. The incorporation of etching steps is shown to decrease the amount of Mo present after a total of 20 and 30 ALD cycles. Dashed lines indicate growth that integrated supercycles of deposition and etching. Solid lines indicate ASALD without ALE supercycles.

Journal of Vacuum Science & Technology A

PLEASE CITE THIS ARTICLE AS DOI: 10.1116/6.0002811

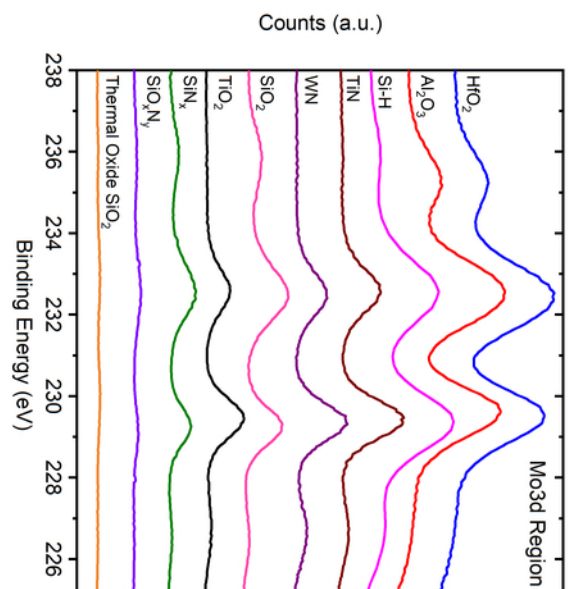

Journal of Vacuum Science & Technology A

PLEASE CITE THIS ARTICLE AS DOI: 10.1116/6.0002811

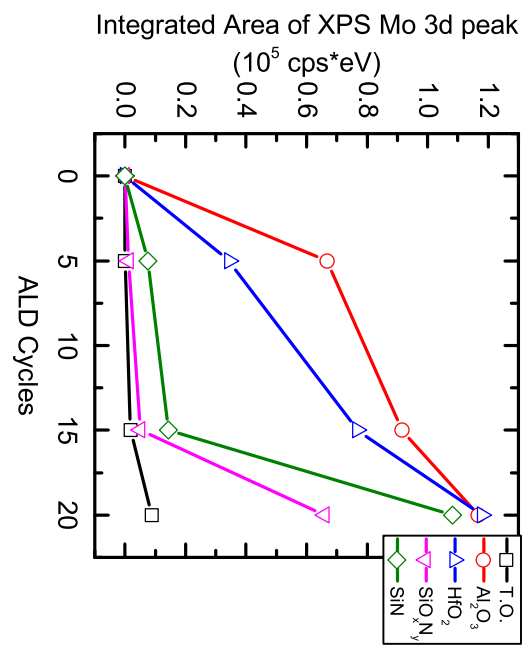

Journal of Vacuum Science & Technology A

PLEASE CITE THIS ARTICLE AS DOI: 10.1116/6.0002811

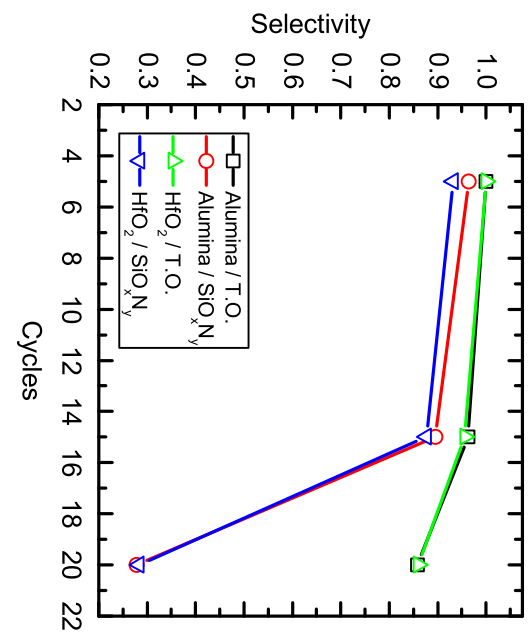

Journal of Vacuum Science & Technology A

PLEASE CITE THIS ARTICLE AS DOI: 10.1116/6.0002811

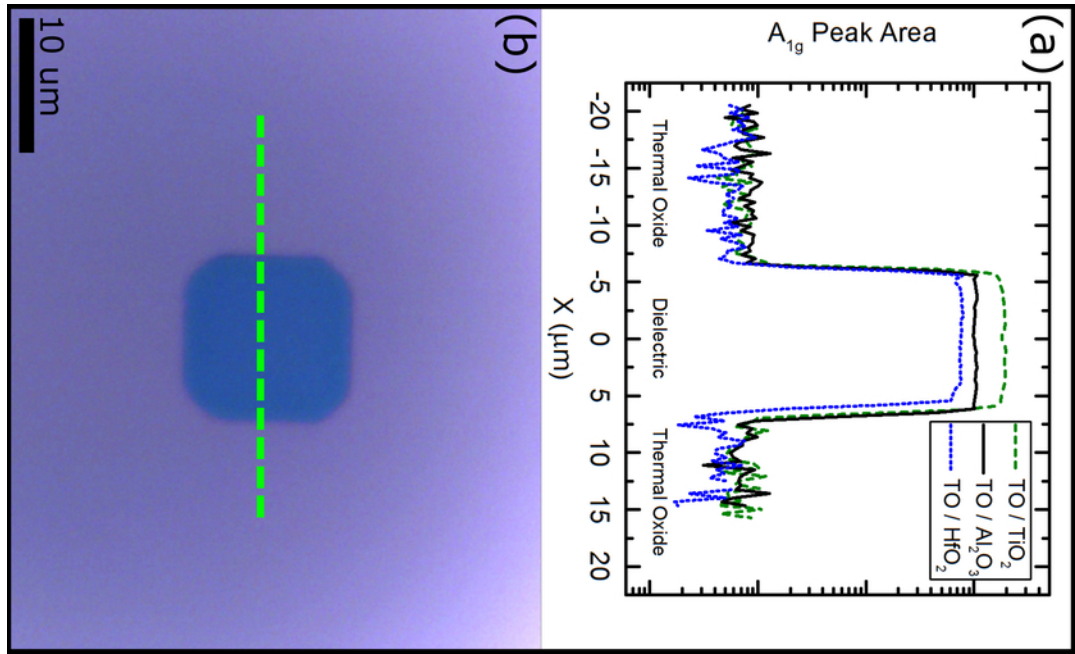

Journal of Vacuum Science & Technology A

PLEASE CITE THIS ARTICLE AS DOI: 10.1116/6.0002811

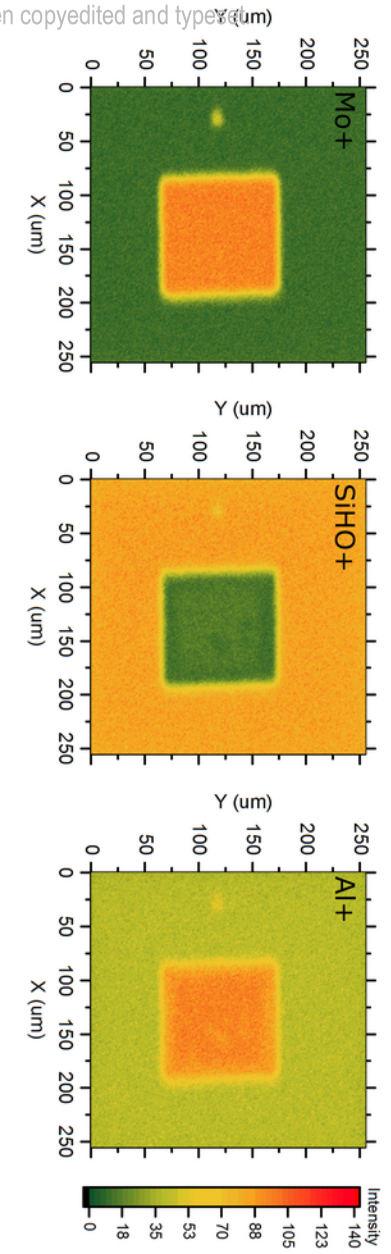

Journal of Vacuum Science & Technology A

PLEASE CITE THIS ARTICLE AS DOI: 10.1116/6.0002811